Geometric characteristic of flexural-shear cracks of members without shear reinforcement

Lu, J.; Yang, Y.; Hendriks, M.A.N.

Publication date
2022

Document Version
Final published version

Published in
The proceedings of the 14th fib PhD Symposium 2022

Geometric characteristic of flexural-shear cracks of members without shear reinforcement

Jiandong Lu[1], Yuguang Yang[1] and Max A.N. Hendriks[1,2]

1 Department of Engineering Structures,
Delft University of Technology,
Stevinweg 1, 2628CN Delft, the Netherlands

2 Department of Structural Engineering,
Norwegian University of Science and Technology,
Richard Birkelands vei 1A, 7491 Trondheim, Norway

Abstract
For reinforced concrete members without shear reinforcement, the shear failure is characterized by the formation of a critical flexural shear crack. Recently experimental observations making use of Digital Image Correlation (DIC) by many researchers suggested the significance of geometric characteristics and kinematic conditions of critical shear cracks in shear failure. However, limited efforts were reported in literature on the quantification of the geometric characteristics of critical shear cracks. This is mainly due to the lack of understanding of the mechanism of how the flexural shear cracks form. In this paper, the available models in literature for the shear crack trajectory and the underlying theoretical assumptions are reviewed first. Those models include the shear crack model proposed by the authors. Next, the shear crack trajectory models are validated using a collection of shear crack patterns based on the DIC data obtained from the shear failure database from Delft University of Technology. The majority of the crack patterns are from full-scale shear tests of deep beams with an effective depth larger than 1.0 m. The comparison helps us to have a basic understanding of how accurate the available flexural shear crack trajectory models can achieve.

1 Introduction

Flexural-shear failure of reinforced concrete members without shear reinforcement remains a very challenging topic even after many theories have been developed [1]-[3]. In these theories, the shear capacity is determined by an individual discrete critical shear crack. For a single critical flexural shear crack, the shear capacity is carried by four mechanisms: the contribution of the uncracked compressive zone, residual tensile strength, aggregate interlock, and dowel action. Aggregate interlock contributes a large portion of the total shear resistance [4]. And it highly depends on the geometric characteristics and kinematic conditions of the critical shear cracks. Therefore, in the past decade, more and more researchers have agreed that the shear crack trajectory significantly affects the shear capacity of the reinforced concrete (RC) members without shear reinforcement [4]. However, only limited efforts have been paid to describe the geometric characteristics of flexural shear cracks in literature. The existing trajectory models for flexural shear crack patterns lack a systematic verification. With the help of the advanced measurement technology Digital Image Correlation (DIC), a more detailed measurement of the crack patterns and kinematic information can be obtained [5]-[7]. Therefore, it creates the possibility of making a comparison between the actual crack pattern and the available models in the literature.

This paper aims to quantitatively verify the existing trajectory models for flexural-shear cracks in RC beams without shear reinforcement. First, the existing models from the literature are briefly reviewed. Then, a database of RC beams without shear reinforcement from Delft University of Technology is used to validate the existing crack trajectory models. Specifically, the equivalent strain field from DIC measurement data is used to extract the geometric characteristics of the cracks. The database consists of full-scale shear tests of deep beams with a height of 1.2 m, and the detailed measurement report can be found in Reference [8]. Finally, the coefficient of determination between the actual and theoretical crack patterns is used to show the effectiveness of the existing models.

2 Existing models for flexural shear crack pattern

2.1 Carpinteri's crack model

Carpinteri et al. [9] proposed an equation for the shear crack trajectory based on experimental observations. In this model, the shear crack trajectory includes two parts as shown in Eq. (1).

$$\Gamma(s)=\begin{cases} x_0 & s\le c \\ x_0+\left(\dfrac{s-c}{h-c}\right)^{\mu}(l-x_0) & c<s\le h \end{cases} \tag{1}$$

Where h is the beam depth, l is the shear span, s is the crack height, c is the reinforcement cover, x is the crack tip horizontal position, x_0 is the crack mouth horizontal position and μ is the exponent of the crack trajectory function. The definitions of parameters can be seen in Fig. 1.

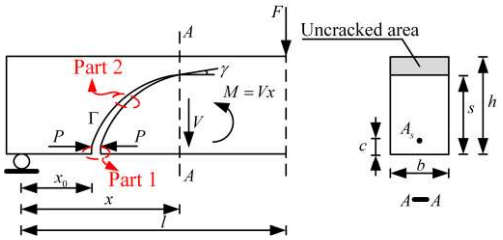

Fig. 1 Definition of parameters used in Carpinteri's model. (Adapted from Reference [9])

In this model, the first part of the crack trajectory model is a straight line, which propagates to the level of longitudinal reinforcement. After that, the crack propagates along an exponential-shaped curved line described in Eq. (1). To describe the geometric characteristic of a crack using Eq. (1), the exponent factor μ needs to be determined. However, the authors did not propose a specific method to determine this factor in the paper, and they proposed to fit the exponent factors μ with experimental data instead [10]. That means the model cannot be a prediction model but rather a description model based on observations. As it is not the main aim of this paper, this model was not used in the comparison.

2.2 Cavagnis's model

Cavagnis et al. [2] proposed another crack trajectory model based on the experimental observations. The basic idea of this model is to divide a flexural shear crack into two straight lines as shown in Fig. 2. In this model, the quantified geometric information of flexural shear cracks is determined by the regression analysis based on test data.

For straight line AB, the angle and the length can be obtained using Eq. (2)-(3), respectively.

$$\beta_{AB}=45°+15°\alpha_A^{1/3}\le 90 \tag{2}$$

$$l_A=d_B/\sin\beta_{AB}=(d-c)/\sin(45°+15°\alpha_A^{1/3}) \tag{3}$$

Where d is the effective depth of the section, c is the height of the compressive zone, and $\alpha_A=M_A/(V_A d)$, with M_A and V_A representing respectively the moment and the shear force in the section at the location of point A.

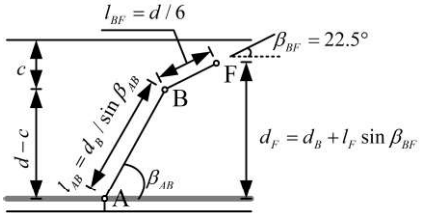

Fig. 2 Crack pattern in Cavagnis's model. (Adapted from Reference [2])

For the secondary branch BF of the flexural shear cracks, the angle is a constant, which equals 22.5 degrees, and the length equals one-sixth of the effective depth. Although the crack trajectory model was derived based on regression analysis of test data, it can capture the most important characteristics of flexural shear cracks.

2.3 Classen's model

Classen [1] developed the Shear Crack Propagation Theory to predict the shear capacities of the reinforced concrete members without shear reinforcement. In this theory, the biaxial stress state at the crack tip of the flexural shear cracks was considered. Furthermore, the angle of principal stress at the crack tip can be calculated, which is perpendicular to the crack propagation angle in a certain step. He used the biaxial failure criterion of concrete to determine the next step of the crack propagation. In this manner, the whole propagation of flexural shear cracks is obtained and the corresponding shear capacity can be calculated as well. His model can be used to obtain a full crack path of a flexural shear crack. However, the model lacks an explicit equation for the crack trajectory and requires complex iterative calculation, which makes a systematic comparison of the model with a large amount of actual crack patterns from different specimens rather challenging. Therefore, the present paper does not include a systematic comparison with this model.

2.4 Yang's model

Yang [3] proposed a crack trajectory model based on fracture mechanics. In this model, the stress state at the crack tip was also considered. Compared to Classen's model [1], Yang used the analytical solution from the failure Mode I (tension) and Mode II (shear) to describe the stress state at the crack tip, which related the stress state to the stress intensity factor. And it is assumed that the crack propagates along the direction perpendicular to the maximum principal stress direction. Based on this assumption, a basic form of the crack path was derived.

$$\frac{d^2x}{ds^2}=\frac{Vd}{M}\psi(\xi,\xi_0,k_c,\frac{c}{h},\frac{M}{Vd}) \tag{4}$$

Where x is the horizontal distance between the crack path and the initial cracking point, s is the crack height, V is the shear force and moment acting in the section at the location of the initial cracking point, M is the corresponding moment, d is the effective depth of the section, and Ψ is a general function including the influence of the beam height h, the concrete cover c, the inclination of stress relief line k_c, the normalized height of stabilized major ξ_0 and the normalized height of a developing crack ξ.

Due to the complexity of the function Ψ, Yang [3] concluded that it is impractical to derive an analytical solution for Eq. (4). To get an explicit equation, Yang used nonlinear finite element method simulations based on Sequentially Linear Analysis (SLA) method proposed by Rots et al. [11]-[12] and Slobbe et al. [13]. Finally, after a series of parametric analyses of the numerical simulations, a semi-theoretical crack trajectory model was derived from the regression analysis of numerical crack paths as shown in Eq. (5).

$$\zeta=\delta_{cr}^{-0.2}\left(\frac{M}{Vd}\right)^{-0.5}\xi^2 \tag{5}$$

Where $\zeta=x/d$ is the normalized coordinate of the crack in the longitudinal direction, $\xi=s/d$ is the normalized coordinate of the crack in the height direction, $\delta_{cr}=l_{crm}/d$ is the normalized crack spacing and the rest of the symbols represent the same meaning as the aforementioned.

Basically, this equation uses a second-order power function to describe the crack path. And it is worthwhile to mention that it includes the influence of generalized span ratio factor $M/(Vd)$ on crack patterns, which shows consistency with both experimental observations and previous theoretical derivations.

3 Development of a crack pattern data set of deep beam tests

To make a systematic comparison between the predicted and the actual crack patterns, a data set including the quantitative information of actual crack patterns is needed. However, such a data set can not be found in the existing literature. To achieve this goal, the present paper creates a data set using the crack patterns of 34 specimens without shear reinforcement from the report in Reference [8]. All the specimens were loaded by a single point with the simply supported condition. The height of the majority of the specimens is 1200 mm and the width of them is 300 mm. The naming rule is explained here to help readers associate the mechanical properties of the beam to the label better. For H401A specimen, the initial letter represents the test series, the first two digits mean the longitudinal reinforcement ratio, the last digit represents the name of the specimen, and the last letter is related to the loading position. Therefore, specimen H401 is the first beam with a reinforcement ratio of around

0.40% in test series H. In this chapter, an algorithm is used to extract the quantitative information of actual crack patterns from the DIC analysis. The main procedure of the algorithm can be seen in the following sections. In total, the data set includes the quantitative information of 126 cracks.

3.1 Detection of crack patterns

The direct output of DIC analysis is the displacement field of the member, then, the strain field is calculated based on the finite element method with a linear 4-nodes element method. In this method, a linear shape function of the displacement field is assumed. Therefore, the discontinuity due to cracking results in some relatively high strain values in the cracking area. The algorithm identifies the crack pattern by detecting the high strain area in the strain field obtained from the DIC analysis. The DIC analysis in this paper was conducted by an algorithm developed by Jones [14]. The input picture size is 8688 by 5792 pixels. Since the main aim is to extract the crack profile, a relatively large subset size of 121 pixels and a step size of 50 pixels are used in the DIC analysis. As an example, the equivalent strain field of specimen H403A is given in Fig. 3 a).

Then, the missing data points due to a large crack width are filled by three times the mean value of the equivalent strain field so that a full equivalent strain field is obtained as shown in Fig. 3 b). Clearly, some noises can be seen in the red box area, which can result in biased detection. To reduce the noise level, a mean value filter is applied. Specifically, the global mean value of the full equivalent strain field is used as a threshold value. When a data point has a value that is higher than the threshold, it is preserved. Although using the global mean value as the threshold value does not have a very solid physical background, the noise level can be reduced and the main geometric characteristic information of major flexural cracks can be preserved as shown in Fig. 3 c).

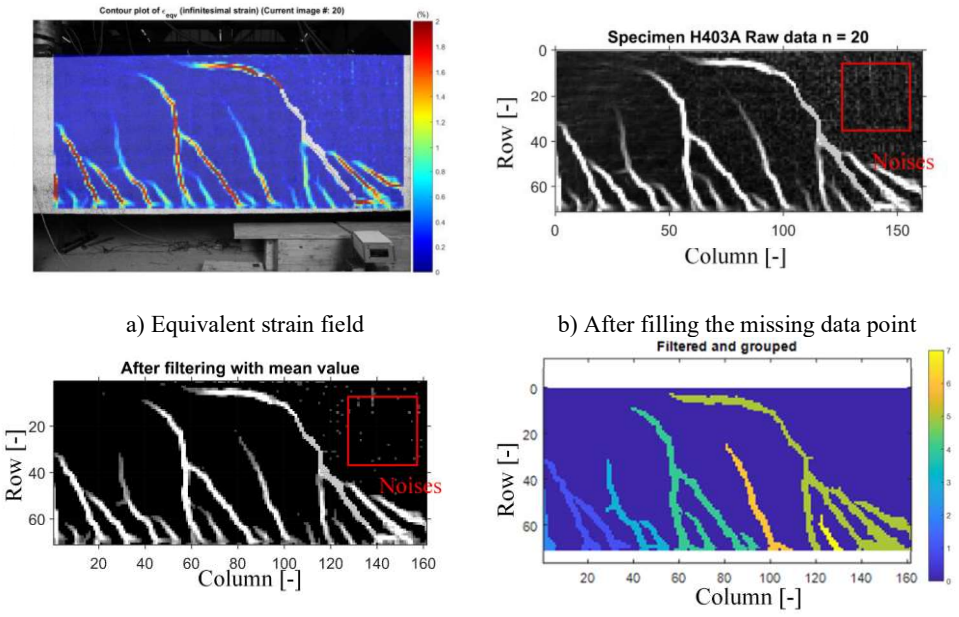

a) Equivalent strain field

b) After filling the missing data point

c) After global mean value filtering

d) After grouping

Fig. 3 Crack pattern detection procedure

The last step is to determine the final crack pattern from the filtered strain field. Here this paper used an algorithm originally developed by Celada [15]. This algorithm provides the function to distinguish different cracks and group them. In this algorithm, firstly, the filtered strain field matrix is converted into a logical matrix. Then, the algorithm divides the high strain area into different groups by judging whether they are connected with each other. To make the detection more robust, two criteria are used to determine whether an individual group can be labeled as a crack instead of a noise area:

The first criterion is the number of pixel points in a group. Since the picture at the moment closed to failure is chosen to extract the crack patterns, the cracks have already developed into a certain height.

It means that a real crack group should include a large enough amount of pixels points, otherwise this group represents a noise area or does not develop into enough height.

The second criterion is the shape formed by all pixel points in a group. Due to the setup of other measurement instruments, some area of the measured surface is blocked by a small steel frame in some specimens. To avoid detecting this steel frame as a crack, this criterion is applied. In the original algorithm, a first-order linear polynomial function is used as a reference, which means that the shape formed by all the pixel points in a single group should have a good approximation compared with a straight line. To achieve this aim, the algorithm follows the next two steps. First, based on the square-least method, a linear regression equation is obtained using the pixel points from one group. Then, the values from the regression function and actual values are used to calculate the coefficient of determination. If the coefficient of determination is larger than a threshold value, this group is categorized as a crack. After observing the shape of the flexural shear crack, this paper uses a three-orde polynomial function as the reference function to increase the robustness of the detection algorithm. The final grouping results can be seen in Fig. 3 d). Although the algorithm can not distinguish the major crack and secondary branches, the majority of well-developed flexural cracks can be detected by this algorithm. After grouping, the data is converted into a point cloud and displayed in the unit of mm.

3.2 Selection of major flexural-shear crack

It is clear that some crack point groups also include the secondary branch while the available crack trajectory models are only for major flexural shear cracks. An algorithm is designed to select the points from the major crack and eliminate the influence of the secondary branch. The general idea of the algorithm is to scan the point cloud of each group from the bottom to the top along a straight line in the longitudinal direction. The scanning procedure starts from the level of longitudinal reinforcement and terminates after reaching the bottom surface of the compressive zone. If the intersection area only includes continuous indexes of points, which means the horizontal scanning line only crosses the major crack, the middle point of the intersection area is selected as the cracking point. When the intersection area includes discontinuous indexes of points, it means the scanning line crosses both the major crack and the secondary branch. For this situation, the first group of points with continuous indexes is considered the major flexural shear crack since the loading point is located on the left-hand side of the image. Then, the corresponding middle point of this group is extracted. The final results can be seen in Fig. 4.

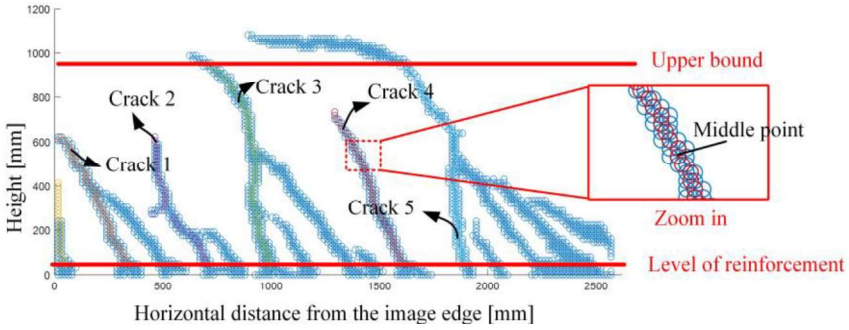

Fig. 4 Selection of the major flexural-shear crack pattern

4 Model validation

4.1 Determination of local generalized span ratio

To obtain the predictive crack patterns based on both Cavagnis's [2] and Yang's [3] model, the *M/Vd* ratio at the initial cracking point should be determined first. It is defined by the intersection point between the major flexural shear crack and the longitudinal reinforcement as shown in Fig. 4. Since the thickness of the concrete cover is known, the intersectional points and their corresponding coordinates in the x-direction can be determined easily. After determining the location of the loading point, the generalized span ratio can be calculated by (6).

To determine the location of the loading point, for the images including the jack, the location can be directly selected from the picture. However, for those pictures without the jacks, the locations were

roughly assumed to be the left edge of the image, which means the corresponding x-coordinate equals 0.

$$\frac{M}{Vd} = \frac{V(a-(x+x_{load}))}{Vd} = \frac{a-(x+x_{load})}{d} \tag{6}$$

Where a is the span ratio, x is the x-coordinate of the intersection point, and x_{load} is the x-coordinate of the loading point.

4.2 Criterion of the comparisons

After obtaining the local generalized span ratio, the full crack pattern can be obtained using Eq. (2)-(3) or Eq. (4), respectively. It should be noted that since only the crack pattern under the compressive zone will be used in the comparisons, the secondary branch described in Cavagnis's model [2] will not be used. Due to the variation and randomness of cracks, it is not practical to verify the models by a single crack. So the rest of the results will be shown in a statistical way. To compare the actual crack patterns and the existing models in a quantitative way, the coefficient of determination was used and it can be calculated by Eq. (8).

$$R^2 = 1 - \frac{SS_{res}}{SS_{tot}} = 1 - \frac{\sum_{i=1}^{n}(x_i - f_i)^2}{\sum_{i=1}^{n}(x_i - \bar{x})^2} \tag{8}$$

Where SS_{res} is the sum of squares of residuals between the prediction values and actual values, SS_{tot} is the total sum of squares, x_i is the x-coordinates of the actual flexural shear cracks, f_i is the x-coordinates of the calculated flexural shea cracks and $\bar{x}$ is the mean value of the coordinates of the actual flexural shear cracks.

4.3 Statistics results

To show the comparison results from the algorithm, two specific specimens H301A and H402A are selected and the results can be seen in Fig. 5 and Fig. 6, respectively. They both fail in flexural-shear failure and have the typical flexural-shear crack pattern. Since the function of the algorithm is to detect the crack patterns and make the comparison, the selection of the specimens does not affect its robustness and generalization. In Fig. 5 and Fig. 6, both models reach a similar level of approximation to the actual flexural shear cracks. Cavagnis's model has a higher coefficient of determination.

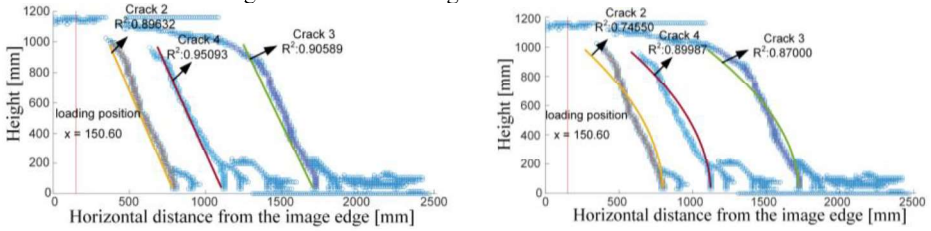

a) Comparison with Cavagnis's model b) Comparison with Yang's model

Fig. 5 Crack pattern comparison of Specimen H301A

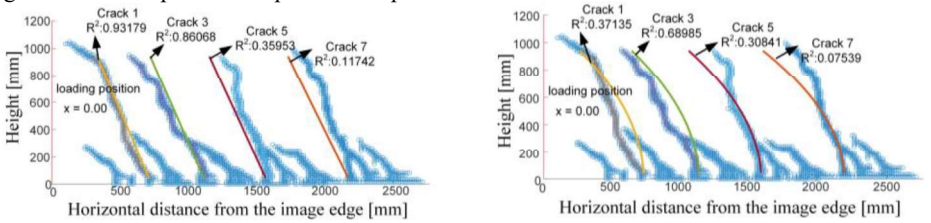

a) Comparison with Cavagnis's model b) Comparison with Yang's model

Fig. 6 Crack pattern comparison of Specimen H402A

Fig. 7 shows the coefficient of determination results against the ratio between the distance from the initial cracking point to the loading point and the average cracking spacing of major cracks. The detailed derivation of average cracking spacing of major cracks can be seen in Reference [3] and the value can

be calculated by Eq.(9). Note that the major cracks mentioned here are the cracks that can develop to a curtained height s_{cr} and the secondary branches toward to the level of longitudinal reinforcement are not considered as a part of the major cracks.

$$l_{crm} = \frac{s_{cr}}{k_c} = \frac{(1+\rho_s n_e - \sqrt{2\rho_s n_e + (\rho_s n_e)^2})d}{k_c} \tag{9}$$

It is very clear that when the ratio is smaller than 1, both models have very poor approximations against the actual crack pattern. Because when the cracks are closed to the loading point, the stress state at the crack tip is highly affected by the localized compression and the cracks are likely to be straight lines rather than curved lines. Both models are only suitable to describe the cracks which are one time of l_{crm} far away from the loading point.

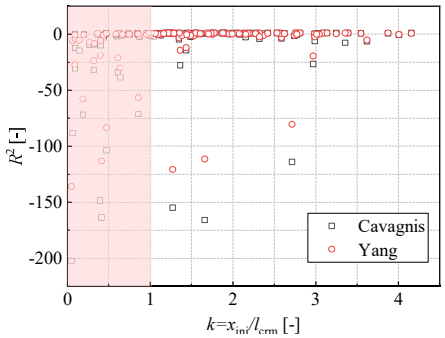

Fig. 7 Coefficient of determination against the ratio between the distance from the initial cracking point to the loading point and the average cracking spacing of major cracks.

After selecting the suitable cracks, only the cracks having positive coefficient of determination are chosen. In this manner, there are 63 cracks in total for Cavagnis's model and 61 cracks for Yang's model. Their statistical histogram results can be seen in Fig. 8. In this paper, when the coefficient of determination is larger than 0.7, we conclude that the calculated results fit the experimental results well. Therefore, for Cavagnis's model, around 60% of the calculated results have an R^2 coefficient larger than 0.7, and around 44% of the calculated results from Yang's model have a coefficient that can exceed 0.7.

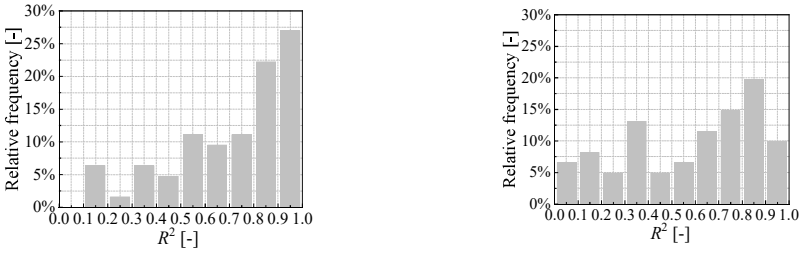

a) Cavagnis's model b) Yang's model

Fig. 8 Histogram results of the coefficients of determination for two models

5 Conclusions

In this paper, the possibility to verify the flexural-shear crack trajectory model using crack patterns obtained from experiments in a quantitative way was explored. And a crack data set using the proposed algorithm has been created. The procedure and the statistical results lead to some conclusions and recommendations as follows.

1) Based on the statistical results, Cavagnis's model and Yang's model both showed poor approximation to the actual crack pattern when the cracks are closed to the loading point. Therefore, it can be concluded that both models have a certain workable range and only the cracks that are one time of l_{crm} away from the loading point can be described by those two models.

2) The statistical results prove that both models can reach a good level of approximation against the experimental crack pattern and Cavagnis's model had a better result. Those two models are suitable for further use in a mechanical shear model to derive the corresponding kinematic model.

3) The current paper only collects the data of some simply supported beams with one depth. To verify the models more systematically, more data from tests of members under different boundary conditions and configurations are needed.

Acknowledgments

The authors wish to acknowledge the experimental data and algorithm support from Zarate Garnica.

References

[1] Classen, M., 2020. Shear Crack Propagation Theory (SCPT)–The mechanical solution to the riddle of shear in RC members without shear reinforcement. *Engineering Structures*, 210, p.110207.

[2] Cavagnis, F., Simões, J.T., Ruiz, M.F. and Muttoni, A., 2020. Shear Strength of Members without Transverse Reinforcement Based on Development of Critical Shear Crack. *ACI Structural Journal*, 117(1).

[3] Yang, Y., 2014. Shear behaviour of reinforced concrete members without shear reinforcement: a new look at an old problem. PhD diss., Delft University of Technology.

[4] Cavagnis, F., Fernández Ruiz, M. and Muttoni, A., 2018. An analysis of the shear-transfer actions in reinforced concrete members without transverse reinforcement based on refined experimental measurements. *Structural concrete*, 19(1), pp.49-64.

[5] Cavagnis, F., 2017. Shear in reinforced concrete without transverse reinforcement: from refined experimental measurements to mechanical models (Doctoral dissertation, Ecole Polytechnique Fédérale de Lausanne).

[6] Gehri, N., Mata-Falcón, J. and Kaufmann, W., 2020. Automated crack detection and measurement based on digital image correlation. *Construction and Building Materials*, 256, p.119383.

[7] Zarate Garnica, G., 2018. Analysis of shear transfer mechanisms in concrete members without shear reinforcement based on kinematic measurements.

[8] Zarate Garnica, G., & Yang, Y., 2018. Measurement report on the shear behaviour of 1.2m deep RC slab strips.

[9] Carpinteri, A., Carmona, J.R. and Ventura, G., 2007. Propagation of flexural and shear cracks through reinforced concrete beams by the bridged crack model. *Magazine of concrete research*, 59(10), pp.743-756.

[10] Carpinteri A, Carmona JR, Ventura G. Failure Mode Transitions in Reinforced Concrete Beams--Part 2: Experimental Tests. ACI Structural Journal. 2011;108.

[11] Rots, J.G. and Invernizzi, S., 2004. Regularized sequentially linear saw-tooth softening model. *International journal for numerical and analytical methods in geomechanics*, 28(7-8), pp.821-856.

[12] Rots, J.G., Belletti, B. and Invernizzi, S., 2008. Robust modeling of RC structures with an "event-by-event" strategy. *Engineering Fracture Mechanics*, 75(3-4), pp.590-614.

[13] Slobbe, A.T., Hendriks, M.A.N. and Rots, J.G., 2012. Sequentially linear analysis of shear critical reinforced concrete beams without shear reinforcement. *Finite Elements in Analysis and Design*, *50*, pp.108-124.

[14] Jones, E., 2015. Documentation for Matlab-based DIC code, Version 4. University of Illinois, Champaign County, Illinois.

[15] Celada Blesa, U., 2019. Theoretical and experimental study of the behaviour at service and failure of partially prestressed concrete beams under flexure and shear. PhD diss. Universitat Politècnica de Catalunya